Doping-induced Ti^{3+} state and oxygen vacancies in TiO_2: a single-chip combinatorial investigation

Raja Elrahoumi,[1] Liangchen Zhu,[1] Estelle Wagner[2], William Maudez[2], Giacomo Benvenuti,[2] Matthew R. Phillips,[1] and Cuong Ton-That[1,*]

[1] *School of Mathematical and Physical Sciences, University of Technology, Sydney, Ultimo, NSW 2007, Australia*

[2] *3D-OXIDES, 41 Rue Henri Fabre, Saint Genis Pouilly 01630, France*

* Corresponding author: cuong.ton-that@uts.edu.au

Abstract

TiO_2 is widely recognized as a high performance photocatalyst for photocatalytic applications. Oxygen vacancies (V_O) and titanium defects are known to make a significant contribution to the enhanced photocatalytic efficiency of TiO_2, accordingly control of these two centers is pivotal to optimizing the surface photochemical activity. In this work, the formation of V_O and Ti^{3+} ions induced by n-type doping of TiO_2 with Nb is demonstrated using a combinatorial investigation approach. Chemical Beam Vapour Deposition (CBVD) is used to fabricate Nb concentration-graded $(Nb_xTi_{1-x})O_2$ anatase films with $0.009 \leq x \leq 0.033$ over a five micrometer length on a single chip. Cathodoluminescence (CL) microanalysis shows the luminescence intensity decreases with increasing Nb concentration; however, the presence of a self-trapped exciton (STE) emission, characteristic of anatase TiO_2, indicates that the Nb incorporation does not affect the structural properties of TiO_2. Notably, the introduction of Nb donors induces the formation of the signature luminescence bands of V_O and Ti^{3+} at 2.05 and 2.60 eV at 80 K, respectively, and their intensities rise by up to 28% with increasing Nb content. The formation of V_O and Ti^{3+} is attributed to the effect of excess electrons locally produced by Nb donor

doping. The thermal activation energies for the STE and defect-related emissions are found to be identical at 32 ± 4 meV, suggesting that that the recombination kinetics is mediated by Nb donors. Significantly, we demonstrate that the near-surface V_O density can be further increased by two different post-growth treatment approaches: (i) remote hydrogen plasma and (ii) low-energy electron beam irradiation (LEEBI), without effecting the valence state of Ti. Our results open opportunities to optimize the photocatalytic properties of TiO_2 by defect engineering.

Keywords: TiO_2; excess electrons; Nd doping; Ti reduction; oxygen vacancies

INTRODUCTION

TiO_2 is a wide bandgap semiconductor with significant applications in photocatalysis, photoreduction of CO_2 and decomposition of organic pollutants in water, perovskite solar cells and Na ion batteries due to its unique chemical properties, band structure and strong oxidizing ability [1-3]. In particular, the demonstration of TiO_2 anodes for effective photocatalytic hydrogen production has led to intensive research on this material [4]. TiO_2 in the anatase phase has a bandgap of ~ 3.2 eV and is transparent in the visible and infrared spectral region, which severely hinders its practical applications in environmental remediation and photocatalysis. One promising approach to overcome this obstacle is high-pressure hydrogenation of anatase TiO_2 nanoparticles, which results in black titania capable of absorbing light in the visible and infrared range [5]. The success of this post-growth treatment to improve the optical properties of TiO_2 for solar photocatalysis has been attributed to multiple effects, including the formation of various defects, such as Ti-H bonds, oxygen vacancies (V_O) and interstitial (Ti_i), and reduction of Ti^{4+} to Ti^{3+}. Although the exact enhancement mechanism is still a subject of considerable debate, it is that clear enhancing the photochemical activity of TiO_2 can be achieved by controlling these defects [6-8]. A common method to tune the electronic and defect structure of TiO_2 is by the incorporation of n-type dopants, for example P or Nb substitution on the Ti site and F substitution on the O site. Theoretical calculations, infrared absorption spectroscopy and

electron paramagnetic resonance show that common donor dopants, Nb_{Ti} and H, as well as intrinsic V_O defects have ionization energies between 10 to 100 meV [9-11]. However, the influence of donor impurities on the physiochemical and defect properties of TiO_2 is poorly understood to date.

Photoluminescence (PL) and cathodoluminescence (CL) are powerful techniques used to investigate defect structure and catalytic surface sites in TiO_2. Anatase TiO_2, in both bulk and nanostructured forms, typically exhibits a broad emission that contains a main emission peak centered at ~ 2.4 eV. This peak has been shown to be independent of post-growth annealing and has been attributed to an intrinsic emission with a large Stokes shift of ~ 1 eV, arising from the recombination of self-trapped excitons (STEs) within distorted TiO_6 octahedra [12-14]. Additionally, two common sub-bandgap emission bands located at ~ 2.1 and 2.6 eV have been assigned to V_O and excitons bound to Ti^{3+} ions, respectively [14-16]. Both V_O and Ti^{3+} are known to be efficient recombination centers in TiO_2 and play an important role in photocatalytic water oxidation [17]. A previous CL investigation of Nb-doped TiO_2 reports two emissions in the 2.4 – 2.7 eV range; however, their relationship with Nb doping is not clearly evident [18]. Herein, the present work describes a detailed investigation into the effect of excess electrons associated with n-type Nb doping on the formation of V_O and the reduction of Ti^{4+} ions in anatase TiO_2. Our results from the investigation into graded Nd-doped TiO_2 films on a single chip provide unambiguous evidence for the correlation between excess electrons and the concentrations of V_O and Ti^{3+}. Moreover, the work demonstrates the utility of ion and electron irradiation for producing V_O and Ti^{3+} defects in TiO_2. These post-growth methods are promising as they provide a means to tailor the surface photoelectrochemical activity TiO_2 to controls its photocatalytic efficiency for bespoke applications.

EXPERIMENTAL DETAILS

Nb-doped TiO_2 thin films were deposited on Si wafers using the Chemical Beam Vapour Deposition (CBVD) technique as described in detail previously [19, 20]. Briefly the deposition was carried out using two liquid precursors of titanium tetraisopropoxide $(Ti(OiPr)_4$ (TTIP) and tetraethoxy(dimethylaminoethoxy) niobium $(Nb(OEt)_4(dmae))$ as shown the schematic in Figure 1(a). These precursors were heated at 32 and 60 ^oC, respectively, for source evaporation. The base pressure of the chamber was 5×10^{-4} Pa. The substrate was kept at 500 ^oC and the chamber pressure was ~ 2×10^{-3} Pa during deposition. X-ray diffraction (XRD) was performed on a Bruker D8 Discover diffractometer using monochromatic Cu Kα radiation. Correlative investigation of the local Nb concentration and its impact on defects was carried out on a single chip using quantitative X-ray microanalysis and cathodoluminescence (CL) spectroscopy. X-ray microanalysis was conducted on a Zeiss EVO LS15 SEM equipped with an Energy Dispersive X-ray (EDX) analysis system. Cathodoluminescence (CL) was performed using a FEI Quanta 200 scanning electron microscope (SEM) equipped a QE65000 Ocean Optics spectrometer and a parabolic mirror for optical collection. Results were compared with undoped anatase TiO_2 powder (obtained from Sigma-Aldrich) to investigate the impact of Nb doping. To investigate the effect of hydrogenation on defects in Nb-doped TiO_2, remote plasma treatment was carried out in atomic H environment for 5 mins using a hydrogen plasma source at room temperature (Trion plasma chamber operated at pressure = 10 mTorr, H_2 flow rate = 20 sccm and plasma power = 150 W). In low energy electron beam irradiation (LEEBI) investigations, continuous irradiation was carried out with an electron beam energy of 10 keV and a beam current of 90 nA, while collecting CL spectra at 6-minute intervals. All CL spectra were converted from the wavelength to energy scale, and corrected to the response of the optical collection system.

RESULTS AND DISSCUSION

Figure 1(a) shows a schematic of the CBVD fabrication setup with the positions of the Ti and Nb precursor sources used to produce the Nb concentration-graded Nb-doped TiO_2 film on a 4-inch Si wafer. The colour intensity variation across the central blue square qualitatively illustrates the Nb concentration gradient across the $(Nb_xTi_{1-x})O_2$ sample. The film thickness is ~590 nm. The 2θ XRD pattern of the film is presented in Figure 1(b), all the peaks can be indexed to the TiO_2 anatase phase structure according to the JCPDS card no. 21-1272. There are no observed XRD peaks corresponding to TiO_2 rutile or brookite phases, which is consistent with the previous finding that Nb doping stabilizes the anatase phase and inhibits its transformation to other TiO_2 phases [21]. No peaks related to Nb oxides are detectable, suggesting that the TiO_2 film possess highly dispersed Nb cations and that Nb substitutes on the Ti site. Substitutional incorporation of Nb on Ti cation sites is expected since Nb^{5+} (r = 0.64 Å) and Ti^{4+} ions (r = 0.61 Å) have similar ionic radii. A line of analysis locations along the flow direction of the Nb precursor on the graded TiO_2 film are selected for correlative analysis of composition-property relationships. Typical SEM images of the $(Nb_xTi_{1-x})O_2$ film at three locations are presented in Figure 1(c, d, e), which show that the film is composed of close-packed rectangular columnar crystals; detailed descriptions of the film structure were provided in our previous studies [22, 23]. The characterization locations A-E, labelled on the SEM image in the inset of Figure 1(f), are equally spaced with center-to-center separation of ~ 1.2 μm. The surface structure is virtually identical at all of the analysis locations, indicating the film morphology is unaltered by varying the Nb doping concentration. Analysis by atomic force microscopy (AFM) imaging also reveals similar surface structures with an identical surface roughness R_a = 5.5 ± 0.5 nm over a 5 × 5 μm^2 area at these analysis positions (AFM images presented in supplementary Figure S1). EDX elemental microanalysis is used to quantify the local Nb x-fraction of the $(Nb_xTi_{1-x})O_2$ film at each analysis point as shown in Figure 1(f),

which reveals the Nb peak gradually decreases in the direction from A to E. The EDX spectra display characteristic X-ray emission peaks corresponding to Ti and O without any impurity peaks other than a Si peak arising from the substrate. EDX analysis using AZtec EDS software (Oxford Instruments) yields a Nb x-fraction of 0.033 ± 0.003, 0.024 ± 0.003 and 0.009 ± 0.002 at location A, C and E, respectively. The decrease in the Nb concentration from A to E over a distance of ~5 mm in the flow direction of the Nb precursor is consistent with the stoichiometric ratio of the precursors in the fabrication [23].

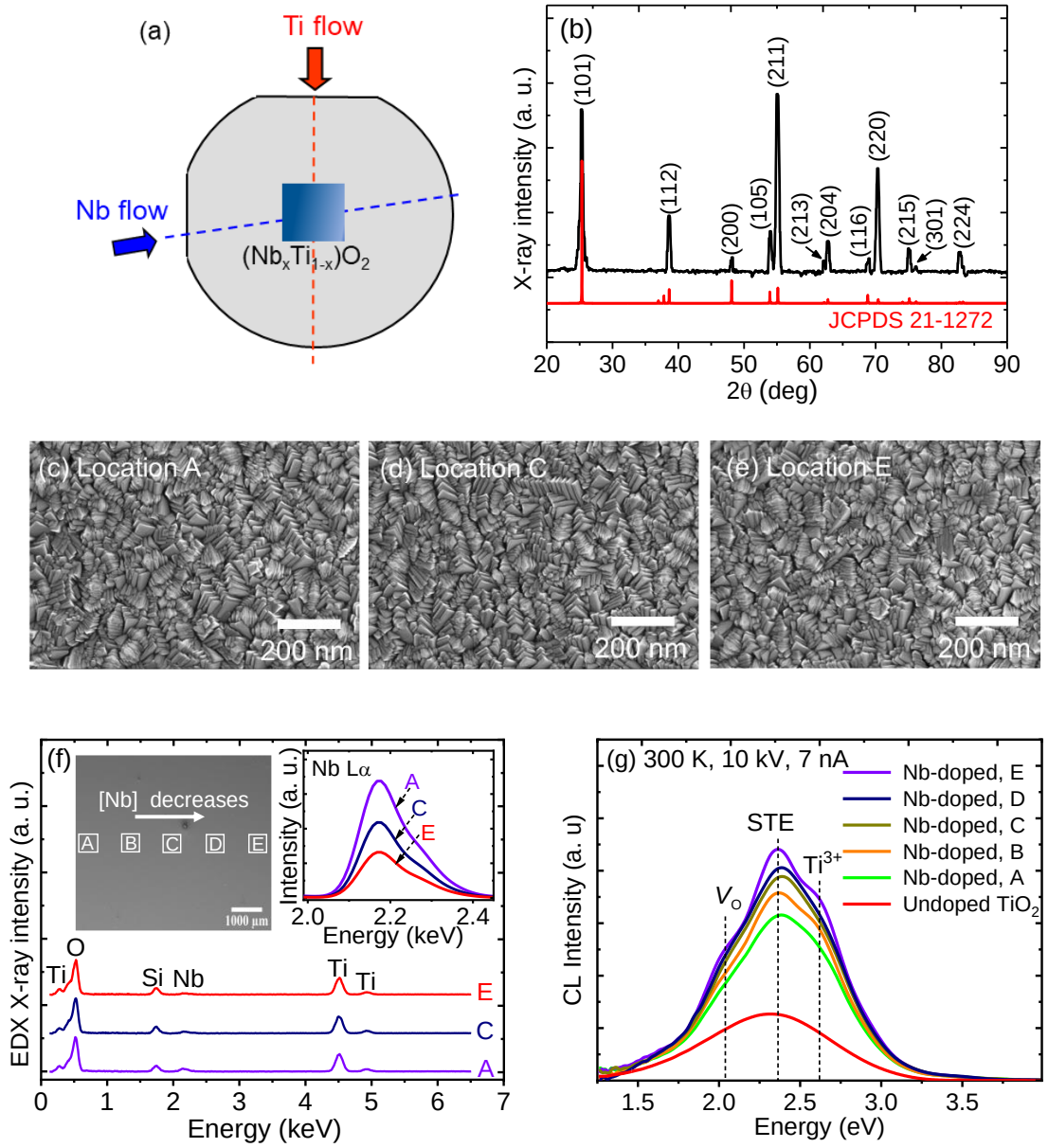

Figure 1. (a) Schematic of the CBVD fabrication to produce a Nb-doped TiO_2 film with the Nb concentration-graded $(Nb_xTi_{1-x})O_2$ sample in the center of the wafer. (b) XRD pattern of the film together with the standard data from JCPDS 21-1272 with all peaks indexed to the anatase phase. (c, d, e) SEM images of the film at 3 locations along the flow direction of Nb precursor, showing similar columnar structures. (f) Representative EDX spectra measured at 10 kV, showing a gradual decrease in the Nb content from x = 0.033 at location A to 0.009 at E (the analysis locations A-E marked in a low-resolution SEM image). Upper right inset shows the Nb Lα EDX peak at 2.17 keV. (f) Corresponding CL spectra acquired at the same acceleration voltage (10 kV) and analysis locations, together with the spectrum of undoped TiO_2, showing the shoulder peaks associated V_O and Ti^{3+} defects due to the Nb incorporation. Both the Nb-doped and undoped TiO_2 exhibit the STE emission at ~ 2.4 eV.

Figure 1(g) shows the CL spectra acquired at 80 K under identical excitation conditions (10 kV, 7 nA) at five locations A-E, which reveals that the CL intensity decreases with increasing Nb concentration. The overall spectral line shape and peak positions are unchanged, indicating the Nb incorporation has a negligible effect on the crystal structure. The reduction in CL intensity with increasing Nb concentration is likely due to the development of defects that act as competitive non-radiative recombination channels; such observation has previously been reported by other authors [24]. As shown in Figure 1(g), the CL spectra of both Nb-doped and undoped TiO_2 are dominated by the intrinsic STE emission at ~ 2.4 eV, which is characteristic of anatase TiO_2 [14, 25]. Compared with undoped anatase TiO_2, the Nb-doped TiO_2 film exhibits a slight blueshift of ~ 54 meV, which can be explained by the Burstein-Moss effect arising from the electron filling of the conduction band (CB) by ionized Nb donors. The Nb-doped film also exhibits two shoulder peaks centered at 2.05 and 2.65 eV, which have previously been attributed to V_O and Ti^{3+} ions, respectively [14, 16]. Both shoulder peaks are absent in the spectrum of undoped TiO_2, indicating the formation of these recombination centers are strongly influenced by the Nb doping. With increasing the local Nb concentration, the two shoulder peaks become more pronounced, indicating higher densities of V_O and Ti^{3+} defects. Notably, the Nb-doped TiO_2 film exhibits no emission in the infrared region below 1.5 eV, which rules out any possible emission associated with interstitial Ti^{3+} [26].

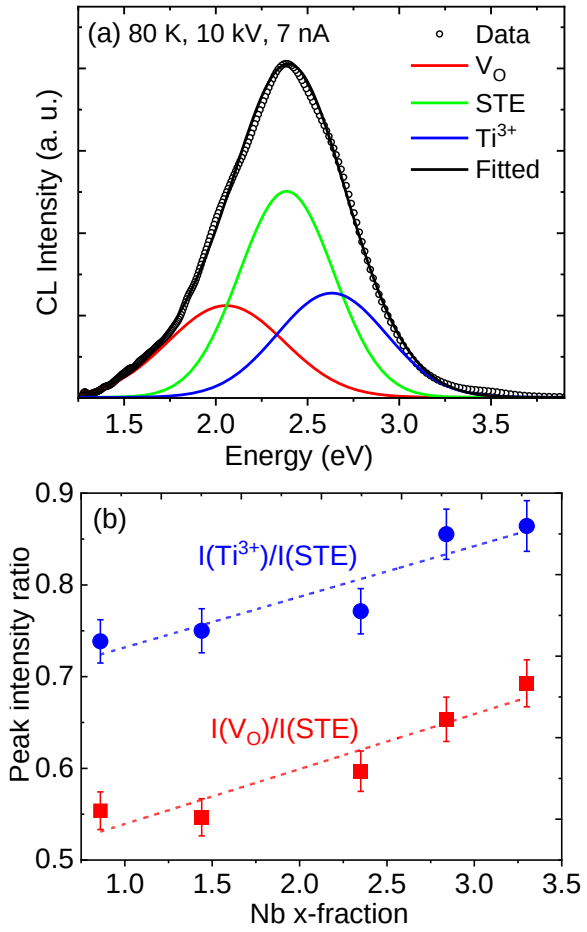

Figure 2. (a) Typical deconvoluted CL spectrum using three Gaussian components representing emission bands associated with V_O, STE and Ti^{3+}. At 80 K, these bands are centered at 2.05 eV (FWHM = 0.57 eV), 2.38 eV (0.51 eV) and 2.65 eV (0.59 eV), respectively. (b) Integrated intensities of V_O and Ti^{3+} defect bands relative to the intrinsic STE emission as a function of local doping Nb concentration. The dashed lines are linear fits to the data.

Both the STE and defect-related peaks in anatase TiO_2 are expectedly broad due to strong electron-photon coupling producing highly overlapped emissions; accordingly spectral deconvolution is needed to extract meaningful results from the luminescence spectra. Curve fitting is made with the position of a main Gaussian peak constrained to the peak of the overall spectrum at 2.38 eV at 80 K as shown in Figure 2(a). This peak represents the intrinsic STE emission in anatase TiO_2. On either side of the STE peak, the spectral line shape is fitted with two broad Gaussian peaks at 2.05 and 2.65 eV and a linear background; these two peaks are

ascribed to the recombination via V_O and Ti^{3+} centers, respectively [12, 14]. This curve fitting approach results in reasonable full width at half maximum (FWHM) values comparable with those reported in the literature [15, 27]. Figure 2(b) displays the integrated intensities of V_O and Ti^{3+} peaks relative to the STE band, which is an intrinsic feature of anatase TiO_2 and independent of defects. (See the integrated intensities of the three emission bands associated with STE, Ti^{3+} and V_O as a function of the Nb x-fraction in Figure S2.) Both the relative peak areas of the V_O and Ti^{3+} bands gradually increase with increasing Nb concentration as explained above. Overall the densities of V_O and Ti^{3+} defects respectively increase by 19% and 28% with increasing the Nb x-fraction in the $(Nb_xTi_{1-x})O_2$ film from x = 0.009 to 0.033. The formation of Ti^{3+} ions can be explained by excess free electrons generated by Nb donors. These delocalized electrons fill empty states at the bottom of the CB and shared by many Ti^{4+} sites, whereas trapped electrons can convert Ti^{4+} ions to the Ti^{3+} state [28]. It is shown theoretically that delocalized and trapped electrons can coexist in the lattice of TiO_2 [28]. The creation of V_O defects with increasing Nb concentration is counter-intuitive since the incorporation of Nb donors would seemingly lead to an increase in the formation energy of V_O donors and hence lower their density. Defect modelling reveals that the V_O formation energy (E_{Vo}) in TiO_2 rises as the Fermi level increases towards the conduction band [29]. However, this dependence between E_{Vo} and the Fermi level does not apply during the non-equilibrium CBVD of the Nb-doped TiO_2 film. Instead, V_O defects are increasingly created as the local Nb vapour is raised because the growth conditions become more cation-rich favouring V_O formation.

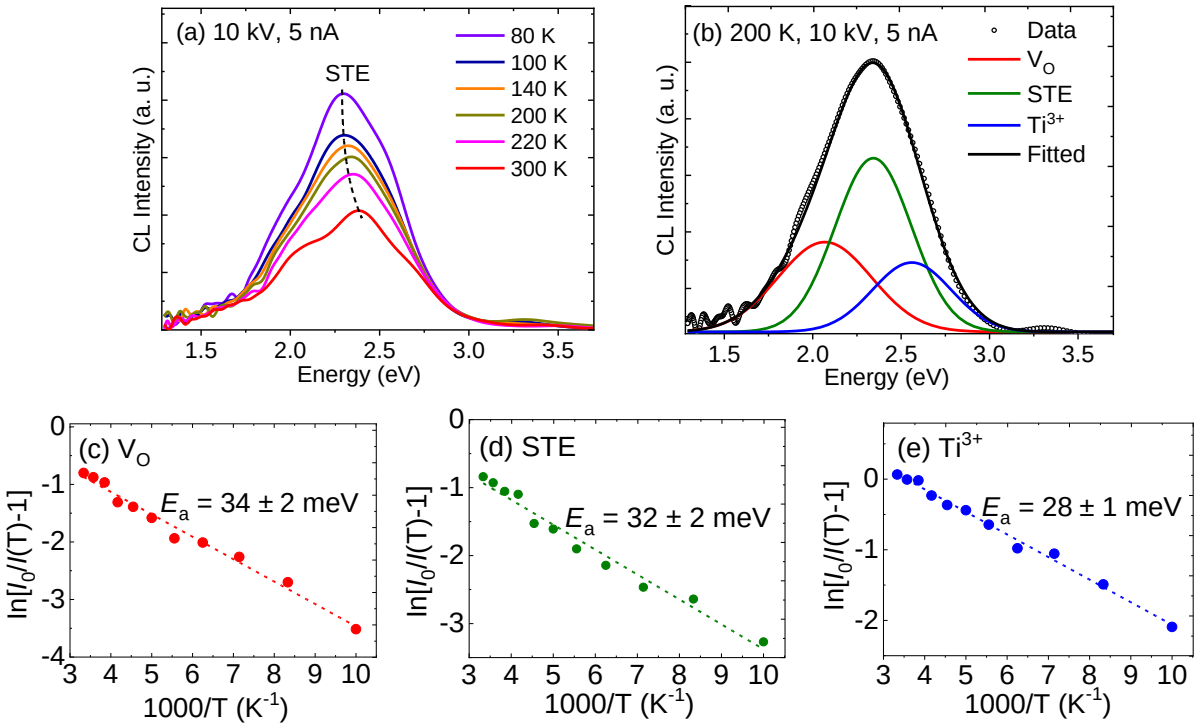

Figure 3. (a) Representative temperature-resolved CL spectra of the Nb-doped TiO_2 film. (b) A typical fitted CL spectrum using 3 Gaussian peaks that are associated with STE, Ti^{3+} and V_O. (c, d and e) Arrhenius plots of ln(I_0/I(T)-1) versus 1000/T and linear analysis using integrated intensities obtained from the curve fitting. The activation energies of the STE, V_O and Ti^{3+} bands are equivalent at E_a = 32 ± 4 meV.

Temperature-resolved CL, performed on location C in the Nb-doped TiO_2 film, is used to investigate the temperature effect on the luminescence properties. The spectra, shown in Figure 3(a), reveal all the three luminescence bands decrease with increasing temperature as competitive non-radiative channels are activated. The STE peak is blue shifted by 105 meV with increasing temperature from 80 K to 300 K. A similar blueshift trend was previously observed in undoped anatase TiO_2 [30]. This behavior in indirect anatase TiO_2 was attributed to the widening of the direct bandgap with temperature due to electron-phonon interactions dominating over thermal expansion contribution [31]. Consequently, a gradual increase in the peak energies of the emission bands with temperature is taken into the curve fitting approach

(see the peak position shifts in Figure S3). An example of the deconvolution to the CL spectrum at 200 K taking into account the blueshift of the STE peak with temperature is presented in Figure 3(b). Arrhenius analysis of the STE, V_O and Ti^{3+} bands is performed to determine the activation energy of their electronic transitions as illustrated in Figure 3(c, d, e). Notably, the activation is found to be identical for the three bands with E_a = 32 ± 4 meV, indicating their recombination kinetics is mediated by a shallow electronic state, most likely the introduced Nb donors. To further probe the characteristics of V_O and Ti^{3+} defects in anatase TiO_2, the FWHMs of their signature emission bands are fitted according to the configuration coordinate model [32]:

$$\mathrm{FWHM} = 2.36\sqrt{S}\hbar\omega\sqrt{\coth\left(\frac{\hbar\omega}{2kT}\right)} \quad [1]$$

where S is the Huang-Rhys factor, and $\hbar\omega$ is the effective phonon energy. The best fit result, shown in Figure S4, is obtained for V_O with S = 6.3 ± 0.4 and $\hbar\omega$ = 38 ± 3 meV, and for Ti^{3+} with S = 7.1 ± 0.6 and $\hbar\omega$ = 28 ± 3 meV. These phonon energies cannot be attributed to any of the known phonon modes in anatase TiO_2 on the basis of Raman data [33] as they represent an average energy of local phonons involved in the optical transition.

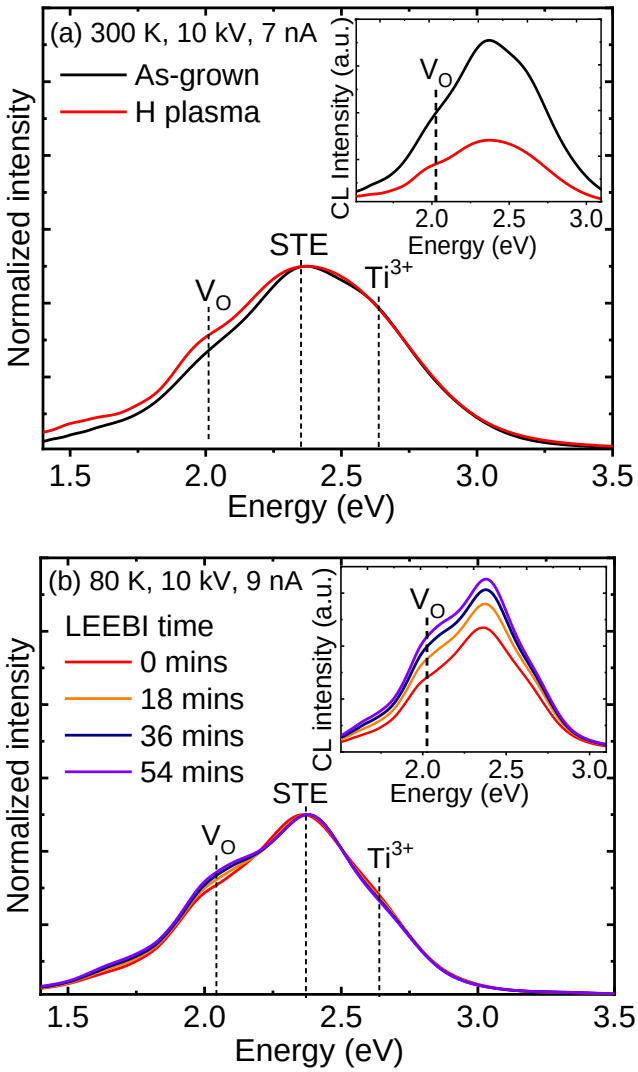

Figure 4. (a) CL spectra of the Nb-doped TiO_2 film normalized to the STE peak before and after H plasma treatment. The relative intensity of the V_O peak increases further by 15% due to the H plasma while the Ti^{3+} emission is unaltered. Inset shows the raw spectra showing the overall CL intensity drops by 60% due to plasma-induced damage to the film. (b) Normalized CL spectra of the LEEBI treated Nb-doped TiO_2 film at various irradiation times up to 54 mins at 80 K, showing a further increase in the relative V_O peak intensity by 12%. Measured CL spectra, displayed in the inset, show the overall emission increases by 38% after LEEBI treatment for 54 mins due to the removal of competitive non-radiative defects.

Now, we turn to the creation of Vo and Ti^{3+} defects using H remote plasma and LEEBI methods. As shown in Figure 4, the spectral line shape and peak positions for the Nb-doped

TiO_2 film are unaltered when it is treated by either H plasma or LEEBI, indicating that these treatments cause no discernible damage to the crystal structure. Figure 4(a) shows the CL spectra of the Nb-doped TiO_2 film normalized to the STE emission peak before and after plasma treatment, which reveals the relative intensity of the Vo peak increases further by 15% due to the H plasma. This result indicates the H plasma is a highly effective treatment to create near-surface V_O defects, while the peak associated with Ti^{3+} ions is unaffected. The measured CL spectra, displayed in the inset of Figure 4(a), shows the overall CL intensity decreases by 60% due to the plasma treatment; such effect has been observed previously and attributed to the formation of near-surface structural defects caused by the plasma exposure [34]. It is known that hydrogen can be trapped at the V_O site and H_O is considered to be more stable than hydrogen interstitials (H_i) in anatase TiO_2 [35]; however, the increase in the V_O density in this work indicates the H remote plasma is an effective approach to extract O atoms from the TiO_2 surface to produce V_O, and a significant portion of these created V_O sites remain as point defects. Previous investigations show V_O defects are generated near the location of Ti^{3+} in reduced TiO_2 in order to maintain charge equilibrium [36]; however, this work demonstrates that the H plasma exposure can efficiently produce V_O without changing the valence state of Ti atoms.

Similarly, for LEEBI treatment, the V_O peak becomes more pronounced upon irradiating with low energy (10 keV) electrons and its relative intensity is observed to further increase by 12% compared with the as-grown film after treating for 54 minutes as shown in Figure 4(b), which displays the normalized CL spectra at various LEEBI times. The LEEBI treatment does not induce any changes to the peak shape and positions of the signature V_O, STE and Ti^{3+} bands as shown in the inset of Figure 4(b) and supplementary Figure S5. Remarkably, the CL emission is found to be monotonically enhanced with increasing LEEBI time due to the formation of a sub-surface electric field induced by charge trapping [37]. Accordingly, the gradual increase in the overall CL emission is attributed to the electric field induced

electromigration of mobile charged defects either into or out of the electron-solid interaction volume [38], which decreases the density of non-radiative defects that compete with the radiative STE, Vo and Ti^{3+} channels. The increase in the intensity of the V_O signature peak due to LEEBI is unexpected because the 10 kV electron beam energy is well below the threshold displacement energy (> 200 keV) for O and Ti atoms in TiO_2 [39]. Hence, the LEEBI exposure cannot create V_O defects by a knock-on mechanism. However, the near-surface V_O concentration can possibly increase during LEEBI by either (i) the outward electromigration of existing charged Vo centers towards the film surface or (ii) the dissociation of weakly bound V_O-related defect complexes by the sub-surface electric field. These results show LEEBI is a possible approach to locally tune the V_O density in TiO_2.

CONCLUSIONS

We demonstrate a growth approach as well as two post-growth methods to generate V_O and Ti^{3+} defects in anatase TiO_2 for the enhancement of photocatalytic properties. Combinatorial investigation of concentration-graded $(Nb_xTi_{1-x})O_2$ films on a single chip shows that doping anatase TiO_2 with Nb induces the formation of V_O and Ti^{3+} defects. X-ray microanalysis and CL characterization of the $(Nb_xTi_{1-x})O_2$ film with spatially varying Nb x-fractions up to $x = 0.033$ reveal the film retains the anatase crystal structure and exhibits characteristics of STEs as in undoped TiO_2. However, the V_O and Ti^{3+} defect densities are found to increase by up to 28% due to excess electrons produced locally by the Nb doping. Further increases in the V_O density in the Nb-doped TiO_2 can be achieved through hydrogen remote plasma treatment and LEEBI, while the valence state of Ti is unaffected by these treatments. These results conclusively indicate that a combination of donor doping and H ion plasma can produce a high concentration of active surface V_O sites for photocatalytic applications.

CRediT authorship contribution statement

Raja Elrahoumi: Investigation, Data curation, Formal analysis, Writing − original draft. **Liangchen Zhu:** Investigation, Data curation. **Estelle Wagner:** Conceptualization, Investigation. **William Maudez:** Conceptualization, Validation. **Giacomo Benvenuti:** Conceptualization, Methodology, Resources. **Matthew R. Phillips:** Methodology, Writing − review & editing. **Cuong Ton-That:** Conceptualization, Formal analysis, Writing − review & editing.

Declaration of competing interest

The authors declare that they have no known competing financial interests or personal relationships that could have appeared to influence the work reported in this paper.

Data Availability

Data will be made available on request.

Acknowledgments

This research was supported under Australian Research Council (ARC) Discovery Project funding scheme (project DP210101146) and the Australian Academy of Technology and Engineering (ATSE) through the Global Connection Fund. The authors would like to thank Herbert Yuan, Curtis Irvine and James Bishop for technical support.

Appendix A. Supplementary data

Supplementary data to this article can be found online at xxx.

References

[1] T. Ali, A. Ahmed, U. Alam, I. Uddin, P. Tripathi, M. Muneer, Enhanced photocatalytic and antibacterial activities of Ag-doped TiO2 nanoparticles under visible light, Materials Chemistry and Physics, 212 (2018) 325-335.

[2] J. Low, B. Cheng, J. Yu, Surface modification and enhanced photocatalytic CO2 reduction performance of TiO2: a review, Applied Surface Science, 392 (2017) 658-686.

[3] Y. Li, J.K. Cooper, W. Liu, C.M. Sutter-Fella, M. Amani, J.W. Beeman, A. Javey, J.W. Ager, Y. Liu, F.M. Toma, Defective TiO2 with high photoconductive gain for efficient and stable planar heterojunction perovskite solar cells, Nature Communications, 7 (2016) 12446.
[4] M. Ni, M.K. Leung, D.Y. Leung, K. Sumathy, A review and recent developments in photocatalytic water-splitting using TiO2 for hydrogen production, Renewable and Sustainable Energy Reviews, 11 (2007) 401-425.
[5] X. Chen, L. Liu, P.Y. Yu, S.S. Mao, Increasing solar absorption for photocatalysis with black hydrogenated titanium dioxide nanocrystals, Science, 331 (2011) 746-750.
[6] H. Xie, N. Li, X. Chen, J. Jiang, X. Zhao, Surface oxygen vacancies promoted photodegradation of benzene on TiO2 film, Applied Surface Science, 511 (2020) 145597.
[7] S. Selcuk, X. Zhao, A. Selloni, Structural evolution of titanium dioxide during reduction in high-pressure hydrogen, Nature Materials, 17 (2018) 923-928.
[8] A. Chatzitakis, S. Sartori, Recent advances in the use of black TiO2 for production of hydrogen and other solar fuels, ChemPhysChem, 20 (2019) 1272-1281.
[9] S. Moser, L. Moreschini, J. Jaćimović, O. Barišić, H. Berger, A. Magrez, Y. Chang, K. Kim, A. Bostwick, E. Rotenberg, Tunable polaronic conduction in anatase TiO 2, Physical Review Letters, 110 (2013) 196403.
[10] P.M. Weiser, C. Zimmermann, J. Bonkerud, L. Vines, E.V. Monakhov, Donors and polaronic absorption in rutile TiO2 single crystals, Journal of Applied Physics, 128 (2020) 145701.
[11] E. Lavrov, Hydrogen donor in anatase TiO 2, Physical Review B, 93 (2016) 045204.
[12] H. Yoo, M. Kim, C. Bae, S. Lee, H. Kim, T.K. Ahn, H. Shin, Understanding photoluminescence of monodispersed crystalline anatase TiO2 nanotube arrays, The Journal of Physical Chemistry C, 118 (2014) 9726-9732.
[13] H. Tang, H. Berger, P. Schmid, F. Levy, G. Burri, Photoluminescence in TiO2 anatase single crystals, Solid State Communications, 87 (1993) 847-850.
[14] S. Battiston, A. Leto, M. Minella, R. Gerbasi, E. Miorin, M. Fabrizio, S. Daolio, E. Tondello, G. Pezzotti, Cathodoluminescence evaluation of oxygen vacancy population in nanostructured titania thin films for photocatalytic applications.(Report), Journal of Physical Chemistry A, 114 (2010) 5295-5298.
[15] G. Pezzotti, A. Leto, S. Battiston, M. Minella, W. Zhu, Cathodoluminescence insights into the ionic disorder of photocatalytic anatase films, Journal of Applied Physics, 111 (2012) 103720-103720-103728.

[16] K. Iijima, M. Goto, S. Enomoto, H. Kunugita, K. Ema, M. Tsukamoto, N. Ichikawa, H.J. Sakama, Influence of oxygen vacancies on optical properties of anatase TiO2 thin films, Journal of Luminescence, 128 (2008) 911-913.
[17] F. Amano, M. Nakata, A. Yamamoto, T. Tanaka, Effect of Ti3+ ions and conduction band electrons on photocatalytic and photoelectrochemical activity of rutile titania for water oxidation, The Journal of Physical Chemistry C, 120 (2016) 6467-6474.
[18] D. Casotti, V. Orsini, A. di Bona, S. Gardonio, M. Fanetti, M. Valant, S. Valeri, Ageing effects on electrical resistivity of Nb-doped TiO2 thin films deposited at a high rate by reactive DC magnetron sputtering, Applied Surface Science, 455 (2018) 267-275.
[19] E. Wagner, W. Maudez, S. Bagdzevicius, C.S. Sandu, G. Benvenuti, Chemical beam vapour deposition technique with Sybilla equipment: Review of main results in its 20-year anniversary, Oxide-based Materials and Devices XII, 11687 (2021) 135-154.
[20] E. Wagner, C.S. Sandu, S. Harada, G. Benvenuti, V. Savu, P. Muralt, Fabrication of complex oxide microstructures by combinatorial chemical beam vapour deposition through stencil masks, Thin Solid Films, 586 (2015) 64-69.
[21] J. Arbiol, G. Dezanneau, J. Cerda, A. Cirera, F. Peiro, A. Cornet, J.R. Morante, Effects of Nb doping on the TiO2 anatase-to-rutile phase transition, Journal of Applied Physics, 92 (2002) 853-861.
[22] G. Benvenuti, Chemical beam deposition of titanium dioxide thin films, École Polytechnique Fédérale de Lausanne, Lausanne, 2003.
[23] C. Sandu, E. Wagner, S. Harada, G. Benvenuti, W. Maudez, M. Jobin, C. Pellodi, P. Muralt, A combinatorial chemical beam vapour deposition approach to tune the electrical conductivity of Nb: TiO2 films via Si co-doping, Thin Solid Films, 615 (2016) 265-270.
[24] D. Wrana, T. Gensch, B.R. Jany, K. Cieślik, C. Rodenbücher, G. Cempura, A. Kruk, F. Krok, Photoluminescence imaging of defects in TiO2: The influence of grain boundaries and doping on charge carrier dynamics, Applied Surface Science, 569 (2021) 150909.
[25] H. Tang, H. Berger, P. Schmid, F. Levy, Optical properties of anatase (TiO2), Solid State Communications, 92 (1994) 267-271.
[26] R. Plugaru, A. Cremades, J. Piqueras, The effect of annealing in different atmospheres on the luminescence of polycrystalline TiO2, Journal of Physics: Condensed Matter, 16 (2003) S261.
[27] T. Sekiya, S. Kamei, S. Kurita, Luminescence of anatase TiO2 single crystals annealed in oxygen atmosphere, Journal of Luminescence, 87 (2000) 1140-1142.

[28] A. Janotti, C. Franchini, J. Varley, G. Kresse, C. Van de Walle, Dual behavior of excess electrons in rutile TiO2, Physica Status Solidi (RRL)–Rapid Research Letters, 7 (2013) 199-203.
[29] S. Na-Phattalung, M.F. Smith, K. Kim, M.-H. Du, S.-H. Wei, S. Zhang, S. Limpijumnong, First-principles study of native defects in anatase Ti O 2, Physical Review B, 73 (2006) 125205.
[30] J. Zhang, X. Chen, Y. Shen, Y. Li, Z. Hu, J. Chu, Synthesis, surface morphology, and photoluminescence properties of anatase iron-doped titanium dioxide nano-crystalline films, Physical Chemistry Chemical Physics, 13 (2011) 13096-13105.
[31] Y.-N. Wu, J.K. Wuenschell, R. Fryer, W.A. Saidi, P. Ohodnicki, B. Chorpening, Y. Duan, Theoretical and experimental study of temperature effect on electronic and optical properties of TiO2: comparing rutile and anatase, Journal of Physics: Condensed Matter, 32 (2020) 405705-405705.
[32] W. Stadler, D. Hofmann, H. Alt, T. Muschik, B. Meyer, E. Weigel, G. Müller-Vogt, M. Salk, E. Rupp, K. Benz, Optical investigations of defects in Cd 1− x Zn x Te, Physical Review B, 51 (1995) 10619.
[33] T. Ohsaka, F. Izumi, Y. Fujiki, Raman spectrum of anatase, TiO2, Journal of Raman spectroscopy, 7 (1978) 321-324.
[34] M. Zakria, T.T. Huynh, F.C. Ling, S.C. Su, M.R. Phillips, C. Ton-That, Highly luminescent MgZnO/ZnO multiple quantum wells for photonics devices, ACS Applied Nano Materials, 2 (2019) 2574-2579.
[35] E.V. Lavrov, I. Chaplygin, F. Herklotz, V.V. Melnikov, Y. Kutin, Hydrogen in single-crystalline anatase TiO2, Journal of Applied Physics, 131 (2022) 030902.
[36] S. Horikoshi, H. Tsutsumi, H. Matsuzaki, A. Furube, A.V. Emeline, N. Serpone, In situ picosecond transient diffuse reflectance spectroscopy of opaque TiO 2 systems under microwave irradiation and influence of oxygen vacancies on the UV-driven/microwave-assisted TiO 2 photocatalysis, Journal of Materials Chemistry C, 3 (2015) 5958-5969.
[37] J. Cazaux, e-Induced secondary electron emission yield of insulators and charging effects, Nuclear Instruments and Methods in Physics Research Section B: Beam Interactions with Materials and Atoms, 244 (2006) 307-322.
[38] L. Weston, C. Ton-That, M. Phillips, Doping properties of hydrogen in ZnO, Journal of Materials Research, 27 (2012) 2220-2224.
[39] H. Gu, G. Li, C. Liu, F. Yuan, F. Han, L. Zhang, S. Wu, Considerable knock-on displacement of metal atoms under a low energy electron beam, Scientific Reports, 7 (2017) 184.